Pacific Northwest
NATIONAL LABORATORY

PNNL-36591

Wrought Aluminum-Cerium Alloys by Shear Assisted Processing and Extrusion

September 2024

Scott A. Whalen
Md. Reza-E-Rabby
Brian K Milligan
Benjamin J Schuessler
Timothy J Roosendaal
Teresa L Lemmon

U.S. DEPARTMENT OF ENERGY

Prepared for the U.S. Department of Energy
under Contract DE-AC05-76RL01830

DISCLAIMER

PACIFIC NORTHWEST NATIONAL LABORATORY
operated by
BATTELLE
for the
UNITED STATES DEPARTMENT OF ENERGY
under Contract DE-AC05-76RL01830

Printed in the United States of America

Available to DOE and DOE contractors from
the Office of Scientific and Technical Information,
P.O. Box 62, Oak Ridge, TN 37831-0062
www.osti.gov
ph: (865) 576-8401
fox: (865) 576-5728
email: reports@osti.gov

Available to the public from the National Technical Information Service
5301 Shawnee Rd., Alexandria, VA 22312
ph: (800) 553-NTIS (6847)
or (703) 605-6000
email: info@ntis.gov
Online ordering: http://www.ntis.gov

PNNL-36591

Wrought Aluminum-Cerium Alloys by Shear Assisted Processing and Extrusion

September 2024

Scott A. Whalen
Md. Reza-E-Rabby
Brian K Milligan
Benjamin J Schuessler
Timothy J Roosendaal
Teresa L Lemmon

Prepared for
the U.S. Department of Energy
under Contract DE-AC05-76RL01830

Pacific Northwest National Laboratory
Richland, Washington 99354

Abstract

Al-Ce alloys have attracted recent interest because of their high thermal stability due to the very low solubility of Ce in the Al matrix. The $Al_{11}Ce_3$ eutectic phase gives excellent strain hardening behavior and moderate high-temperature strength in the as-cast state. However, its strengthening effect is limited by its coarse as-cast structure. Therefore, alternative manufacturing methods such as additive manufacturing or equal channel angular pressing have been applied to refine the $Al_{11}Ce_3$ phase to good effect. However, these techniques are both expensive and time-consuming. Therefore, this study aims to use Shear Assisted Processing and Extrusion (ShAPE), an emerging solid phase processing technique that is more easily scalable than the previously mentioned methods. ShAPE can produce useful cross-sections of an Al-8Ce-4Mg alloy while refining the $Al_{11}Ce_3$ phase to produce a higher strength material. It was found that a low temperature ShAPE process can improve the room temperature yield strength by ~60% compared to a binary Al-4Mg alloy. Additionally, the high-temperature yield strength of the Al-Ce alloys increased by 20%, with a simultaneous 15% improvement in ductility compared to the binary Al-Mg alloy. These results highlight the potential for ShAPE as a processing technique for Al-Ce alloys.

Acknowledgments

This research was supported by the Technology Commercialization Fund (TCF) Laboratory Directed Research and Development (LDRD) Program at Pacific Northwest National Laboratory (PNNL). The authors thank Eck Industries for providing feedstock materials and David Weiss for material property data. The authors also thank Anita Waller and Tianhao Wang (PNNL) for editing and proofreading of this manuscript. Microstructural samples were prepared by Angel Ortiz (PNNL). PNNL is a multi-program national laboratory operated for the U.S. Department of Energy (DOE) by Battelle Memorial Institute under Contract No. DE-AC05-76RL01830.

1.0 Introduction

Al-Ce alloys are a new class of aluminum alloys that were specifically designed for high-temperature applications. Ce has a maximum solubility of 0.01 at% in aluminum [1,2], so very little coarsening occurs even at temperatures >350 °C [3]. However, the Al-Ce phase does not provide a high yield strength to the alloy since the low solubility means that very little precipitation occurs, and tertiary elements are normally added for additional strengthening [4,5]. In this work, Al-Ce-Mg was used because of the high-temperature capability of solid solution strengthening from Mg [6].

This class of Al-Ce alloys for elevated temperature applications were originally developed in the form of casting alloys [7,8]. These alloys were high in Ce (up to 16%), which provided a good mushy zone for high castability. However, the $Al_{11}Ce_3$ eutectic phase was quite coarse in these cast alloys, and the strength of the binary alloys was quite low. Therefore, either Ni, Si or Si + Mg were added for precipitation strengthening with Al_3Ni, $Ce(Si_{1-x}Al_x)_2$, and/or Mg_2Si, and solid solution strengthening with the Mg.

These additions improved the strength of the alloys considerably.
However, these precipitates do not have the same thermal stability as the $Al_{11}Ce_3$ phase. Therefore, for high-temperature applications, other strengthening mechanisms must be used. One mechanism is to refine the eutectic microstructure. There are two commonly applied methods to do this: plastic deformation [9,10], and rapid solidification [11]. One method for rapid solidification that is industrially relevant is laser- or electron beam-powder bed fusion additive manufacturing [4,12]. Extensive refinement of the Ce-containing phases occurred, which led to an increase in yield strength of up to 30% compared to cast material. Even after the refinement, however, the yield strength was still relatively low compared to commercial Al alloys.

The other refinement method of plastic deformation has been done on Al-Ce alloys using a few different methods: conventional extrusion, cold rolling, equal channel angular pressing (ECAP), and conventional extrusion [13–15]. Due to the low solubility of Ce and the high strength of the $Al_{11}Ce_3$ intermetallic [2], the high-temperature flow stress of the alloy is much higher than conventional Al extrusion alloys, and the ductility at high temperature is also limited. During extrusion, it was found that the Ce-containing particles were broken up and much more evenly distributed through the matrix and had a considerably higher hardness [13]. Cold rolling also appears to be a viable processing technique for breaking up coarse $Al_{11}Ce_3$ particles [14]. In that study, an Al-9Ce alloy underwent cold rolling and annealing, which reduced the eutectic secondary dendrite arm spacing by 20% and nearly doubled the yield strength without sacrificing ductility. ECAP has also been applied to Al-Ce alloys [15]. The severe plastic deformation from ECAP acted to break up the $Al_{11}Ce_3$ particles, reducing their length and thickness by a factor of 2-4. The yield strength of the alloy more than doubled after 2 passes of ECAP compared to the as-cast alloy. These studies show that that plastic deformation is an effective way of increasing strength in Al-Ce alloys. Each has limitations, however. Conventional extrusion is limited to a low Ce concentration [13], cold rolling is limited to sheet form, and ECAP has issues with scalability and material loss [16].

Therefore, another plastic deformation technique will be investigated here. The technique that will be used in this study intends to apply plastic deformation to refine the microstructure with an emerging manufacturing method called Shear Assisted Processing and Extrusion (ShAPE) [17]. ShAPE is a technique that combines the linear ram motion of conventional extrusion with a rotating die to add additional shear. A schematic of the process is shown in Figure 1. This technique has several advantages over conventional extrusion and ECAP. The first is that ShAPE is scalable and is being commercialized at an industrial level. Extrusion studies with aluminum and magnesium alloys have been carried out with up to 50 mm outer diameter thin-walled tubing that retain good mechanical properties [18,19]. Another advantage is that the shear from the rotating die acts to plasticize the material, allowing for much easier extrusion of difficult-to-extrude materials [20]. An example of this is that alloy 7075 could be extruded at 10 times the speed of conventional extrusion, without homogenization prior to extrusion [21,22]. The final relevant advantage of ShAPE is that the plastic deformation acts to break up large particles such as the $Al_{11}Ce_3$ particles, often improving ductility and/or strength. This has been demonstrated in previous studies with high Fe 6063 [23] or high Si mixed Twitch scrap [24], where large α-$Al(FeSi)_x$ or Si particles were refined and dispersed, and the ductility of the alloys were comparable to 6061 and 6063, even with high tramp element content. These aspects combine to demonstrate ShAPE is a well-suited technique for producing extrusions of Al-Ce alloys.

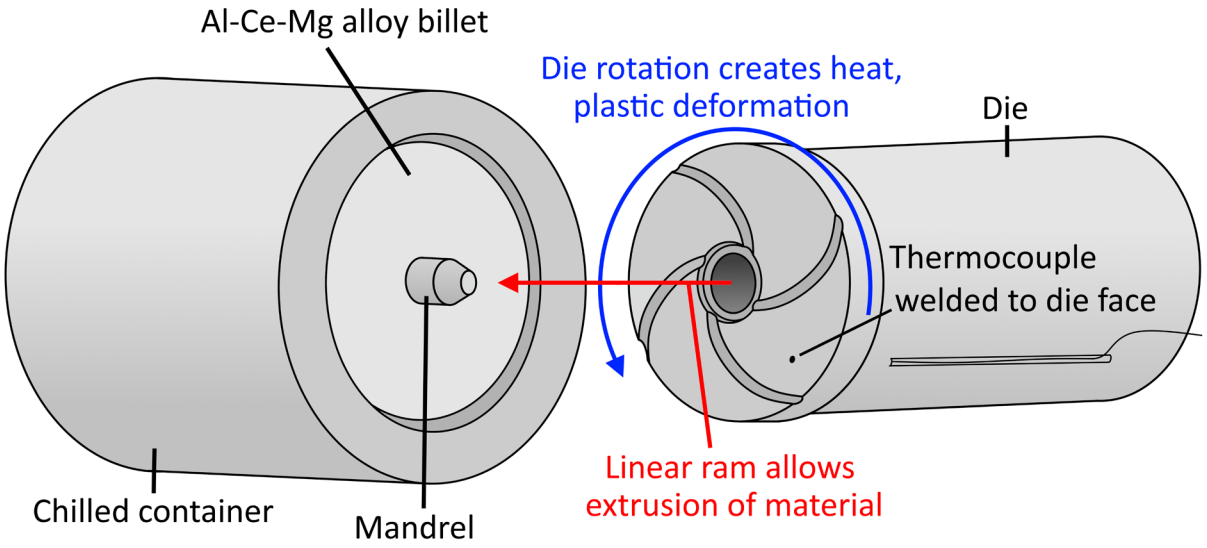

Figure 1: Schematic of the ShAPE process and tooling configuration.

In this study, ShAPE will be used to extrude thin-walled tubing from an as-cast Al-8Ce-4Mg alloy, with varying process parameters. Microstructure will be studied using scanning electron microscopy (SEM), and mechanical properties will be measured by tensile testing. The main goal of the study is to explore the viability of using ShAPE to extrude Al-Ce-Mg tubes, and to understand the effect of process parameters such as temperature and extrusion speed on the microstructure and mechanical properties.

2.0 Materials and Methods

Al-Ce-Mg alloys were provided by Eck Industries via gravity casting into a steel mold with a nominal composition of 8% Ce and 4% Mg with balance of aluminum. The composition was measured using inductively coupled plasma optical emission spectroscopy (ICP-OES) and was found to contain 4.13 wt% Mg, 8.44 wt% Ce, and balance Al with no other elements detected in a significant quantity. These castings were then machined into cylindrical billets with an outer diameter of 31.8 mm, inner diameter of 10 mm, and a length of 101.6 mm.

The billets were then extruded in the as-cast condition using ShAPE over a range of die rotation rates and ram speeds. The extrudate had an outer diameter of 12 mm and an inner diameter of 10 mm, for an extrusion ratio of 20.4. Rotation rate and ram speed were set manually to control the other parameters. Rotation rate primarily determines temperature, and ram speed and rotation rate equally determine advance per revolution (APR). Temperature, ram force, and spindle torque were measured during the experiment. Temperature was measured using a type K thermocouple welded to the die face. Ram force was measured using load cells built into the ShAPE machine. Spindle torque was measured indirectly through the power draw of the spindle motor. A matrix of experiments with varied temperature and APR was performed, and the parameters are displayed in Table 1.

Table 1: Process parameters for each ShAPE experiment. APR refers to advance per revolution and S.S. Temp. refers to steady-state die face temperature.

Trial #	Rotation Rate (RPM)	Ram Speed (mm/min)	APR (mm)	S.S. Temp. (°C)	Max Force (kN)	Max Torque (N·m)
1	70	30	0.4	520	102	43
2	50	120	2.4	520	255	104
3	80	240	3.0	525	360	112
4	35	120	3.4	475	425	156
5	30	120	4.0	425	570	208

The elevated temperature tensile tests were performed using an MTS 312.21 universal testing machine with an MTS 651 environmental chamber and viewing window. Digital image correlation was performed through the window to measure the strain over the specimen gauge length. The tests were run at a constant displacement rate of 3.8mm/min to give an initial strain rate of 0.05/min. Four tests were run for each extrusion.

To observe the microstructure, as-cast billets and tubes were cross sectioned and then mechanically polished to a 0.05μm finish using colloidal silica. Scanning electron microscopy was performed using a JEOL 7600 field-emission scanning electron microscope followed by electron backscatter diffraction using an Oxford Instruments Symmetry detector coupled with the AZtec NanoAnalysis Software, version 6.0. Fully automated large-area mapping was performed using an accelerating voltage of 20 kV, a specimen tilt of 70.0°, and a working distance of ~24.20mm. Indexing of the aluminum

phase was performed using a cubic crystal system, space group (225), Laue group ($Fm\bar{3}m$), with lattice parameters for aluminum a = b = c = 4.04 Å and α = β = γ = 90°, and the Al_4Ce phase using a tetragonal crystal system, space group (139), Laue group (4/mmm), with lattice parameters a = b = 4.37 Å, c = 10.12 Å and α = β = γ = 90°. Cleanup of the EBSD scans and montages were performed utilizing wild spike elimination and a medium level of zero solution extrapolation using the AztecCrystal v2.2.302 software.

3.0 Results

The ShAPE experiments were conducted according to the parameters in Table 1, which resulted in successful extrusions in all cases. Figure 2 shows images of extruded tubes with low APR from Trial 1, and with high APR from Trial 4. Note that the die marks visible on the surface correspond closely with the twist rate and therefore with the APR.

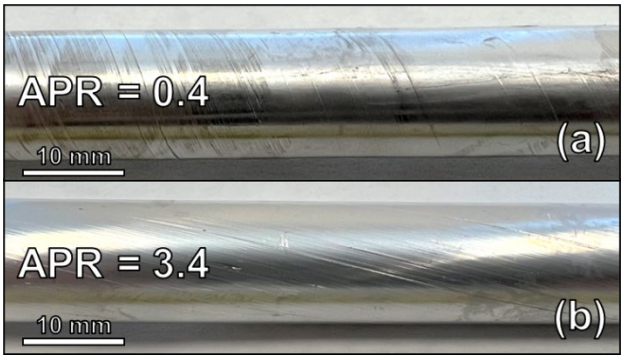

Figure 2: Picture of (a) a low APR tube (Trial 1) and (b) a high APR tube (Trial 4).

Representative stress-strain curves from the tensile tests at room temperature and 250°C are shown in Figure 3. The mechanical property and grain size measurements taken from these specimens are shown in Table 2, along with comparisons against conventional extrusion of similar and identical alloys. Values given are the average of four tensile tests taken from each extrusion. The ± values represent standard deviations between the four tests. Note the large degree of strain hardening in the room temperature tests for all specimens, which is likely caused by the high-volume fraction of unshearable precipitates. Also of note is the high ductility at 250°C seen in all conditions, but especially Trials 4 and 5. This high ductility may be evidence that any large, brittle particles had been refined by ShAPE to the point that they do not cause brittle failure at elevated temperature.

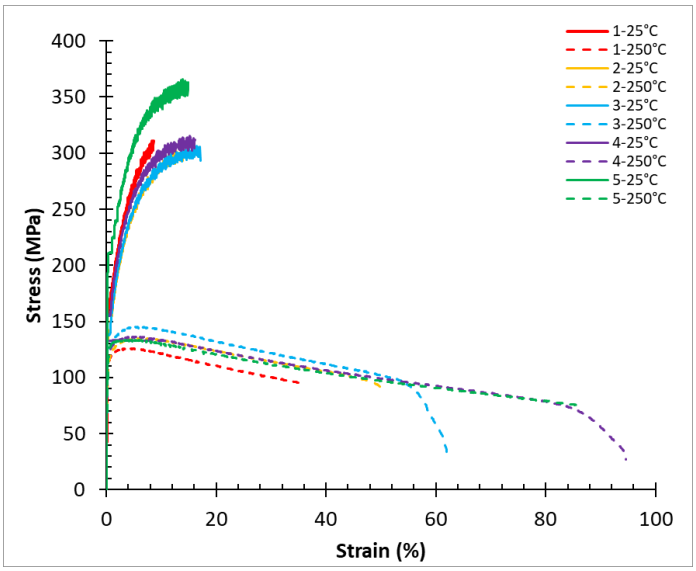

Figure 3: Stress-strain curves for each of the tensile tests at room temperature and at 250°C.

Table 2: Average mechanical properties of each of the trials at room temperature and 250°C. Error is represented as standard deviation between four specimens taken from one extrusion. Binary Al-Mg alloy data at comparable strain rates is also included for comparison. Data for conventional extrusion of an identical alloy is given in the last row.

Trial #	APR (mm)	Die Temp. (°C)	Grain Diameter (μm)	Testing Temp. (°C)	Yield Strength (MPa)	UTS (MPa)	Elongation at Break (%)
1	0.4	520	4.78 ± 3.67	23	152 ± 12	306 ± 15	11 ± 2.3
				250	114 ± 0.5	125 ± 1.3	29 ± 6.4
2	2.4	520	9.18 ± 6.11	23	140 ± 3.1	300 ± 4.7	17 ± 3.7
				250	109 ± 4.2	130 ± 2	70 ± 27
3	3	525	8.77 ± 5.89	23	141 ± 5.4	296 ± 25	15 ± 6.5
				250	110 ± 4	133 ± 5.1	85 ± 20
4	3.4	475	8.51 ± 4.26	23	155 ± 7.4	312 ± 11	18 ± 3.1
				250	112 ± 2.8	130 ± 0.5	95 ± 3.6
5	4	425	6.38 ± 2.85	23	213 ± 2.3	356 ± 13	14 ± 0.9
				250	118 ± 2.4	129 ± 2.4	90 ± 5.8
Al-4wt% Mg [25]				25	128	134	30
Al-4.3wt% Mg [26]				250	98	114	78
Al-8Ce-4Mg [27]				260	61	121	35

The microstructure of the specimens in the as-cast form compared to an example of the ShAPE-processed form from Trial 5 is shown in Figure 4. EDS maps are also included for phase identification in (c-e). Note that in the extruded material, there are large, blocky Ce particles that are slightly refined from the casting and their aspect ratio has been reduced. Also note the light-colored particles in the extrudate that are significantly refined compared to the casting. A banded structure of fine precipitates can also be observed in (b, d) with an appearance similar to stingers in conventional extrusion, with the bands oriented parallel to the extrusion direction. It can also be observed (e) that the Mg is not present in most of the particles and appears to mostly be in solid solution.

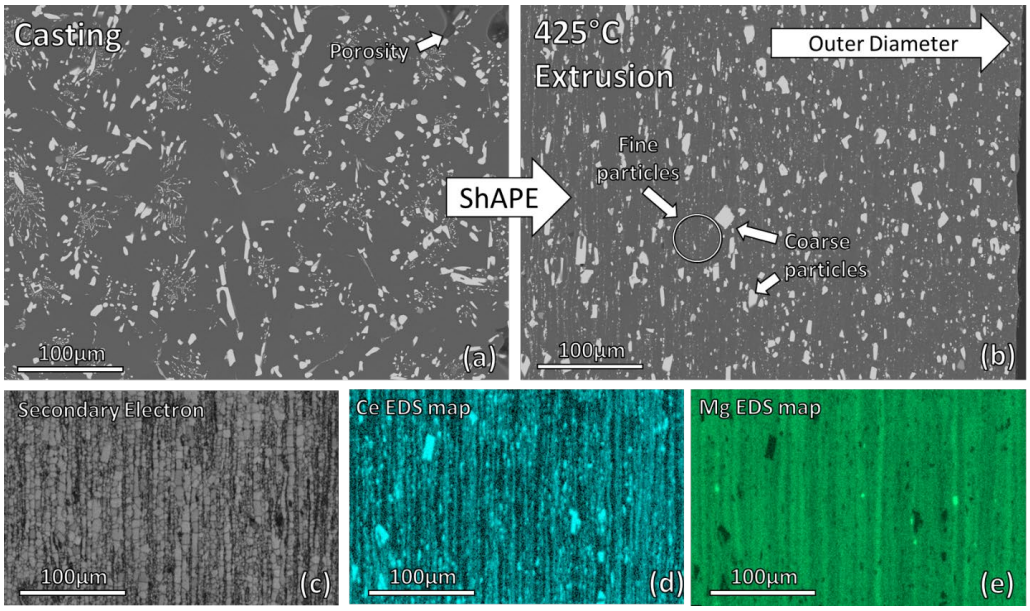

Figure 4: (a-b) SEM-Backscatter images of the as-cast Al-Ce-Mg material versus the extrudate from Trial 5. (c) Secondary electron image, (d) Ce EDS map, and (e) Mg EDS map of the extruded material from Trial 5.

The influence of processing parameters on microstructure is shown in Figure 5. The grain size was also measured using EBSD and is shown in Table 2. It appears that the grain size has an inverse correlation with both temperature and APR with finer grain size produced at lower temperature and higher APR.

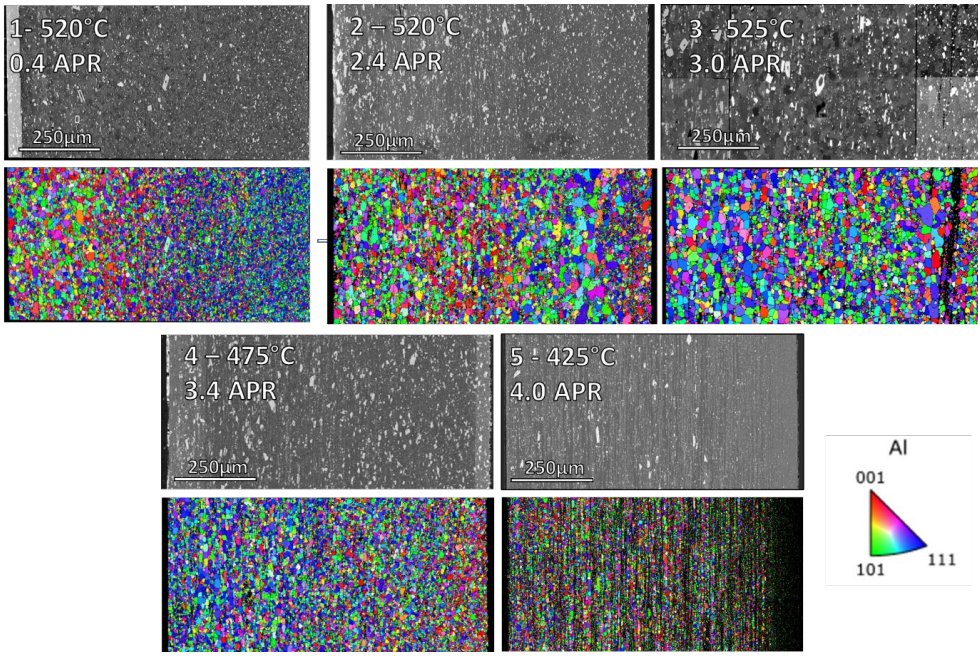

Figure 5: Montaged SEM-backscatter and EBSD IPF-Z maps for the extruded material as a function of extrusion temperature and APR. The outer edge of the extruded tube is on the right side.

4.0 Discussion

The most important variables in determining the mechanical properties was found to be the die face temperature and the APR. To visualize the effect of these variables, they are plotted against the mechanical properties in Figure 6. To isolate the effect of each variable, the other was kept relatively constant (APR=3-4 for f(T) and T=520-525°C for f(APR)), with (a-c) displaying properties as a function of temperature and (d-f) displaying properties as a function of APR. As can be seen, the die face temperature had a strong negative correlation on the yield strength and UTS at room temperature but only a weak effect on the elevated temperature yield strength, no effect on elevated temperature UTS, and no effect on the elongation at either temperature. The APR, on the other hand, had the opposite effect. It had little impact on the strengths at either temperature, but it had a strong positive correlation on the elongation at elevated temperature.

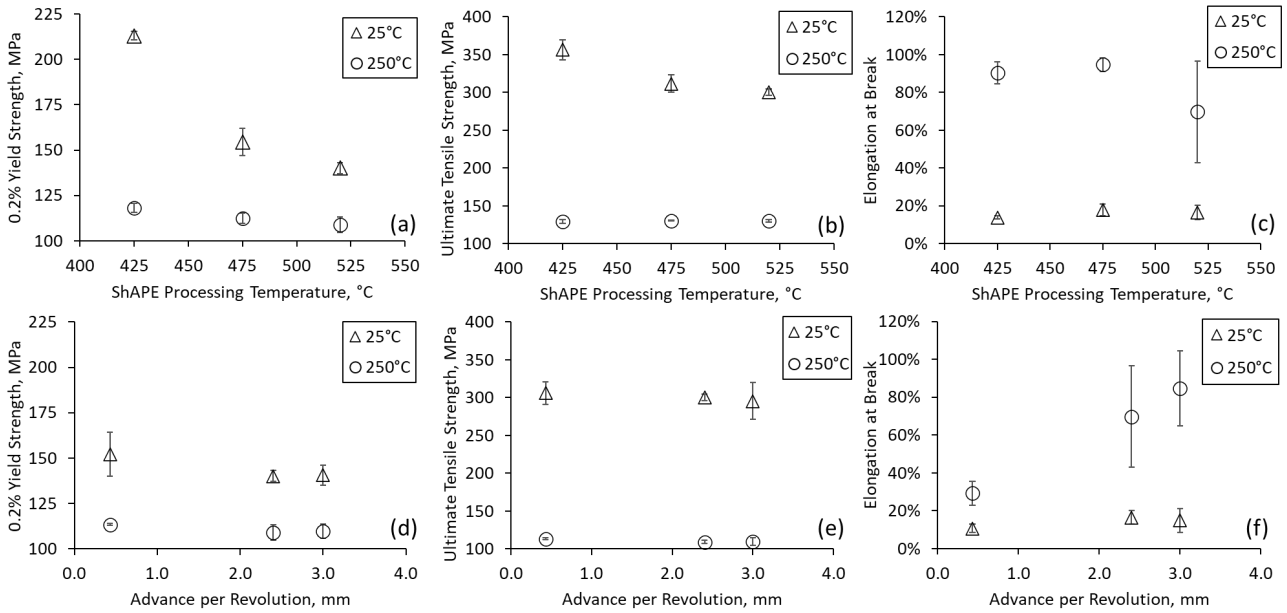

Figure 6: Average yield strength, ultimate tensile strength, and elongation at break shown as a function of die face temperature (a-c) or advance per revolution (d-f). Data is displayed from room temperature testing (triangles) as well as testing at 250°C (circles).

The mechanisms by which the strength is dependent on processing parameters can be elucidated from Figure 5 and Table 2. The higher yield strength and UTS of the Al-Ce-Mg alloy at room temperature compared to the binary Al-4Mg shows that the $Al_{11}Ce_3$ particles are effective in strengthening the alloy. There is also a higher degree of strain hardening in the Al-Ce-Mg alloys than the Al-Mg. The dominant strengthening mechanism that the $Al_{11}Ce_3$ particles provide has been identified in a similar alloy and microstructure to be load transfer strengthening due to its relatively large size and high strength [14]. Due to the refinement of the particles, Orowan strengthening may also be in significant effect. The increase in yield strength as a f(T) can be attributed from the refinement of the $Al_{11}Ce_3$ particles that occurs during low temperature ShAPE processing, which is especially apparent in sample 5. A higher magnification example of the refinement that can be

observed is shown for samples 2 and 5 is shown in Figure 7 for comparison. To quantify the refinement, threshold particle analysis was done using the images shown in Figure 7, with >500 particles analyzed per condition. It was found that reducing the temperature from 520°C to 425°C reduced the $Al_{11}Ce_3$ particle length from 1.83µm to 1.39µm (32%) and the width from 0.93µm to 0.67µm (38%).

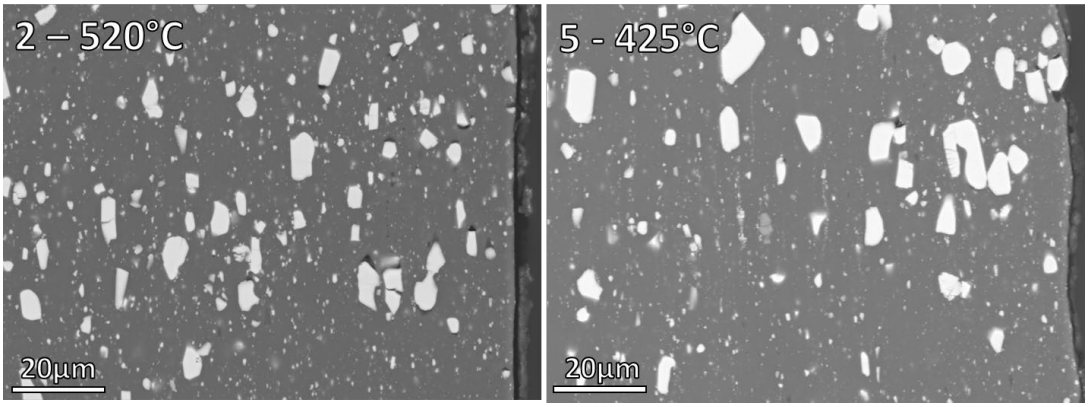

Figure 7: High magnification SEM-BSE comparison of the $Al_{11}Ce_3$ particle structure in Sample 2 (525°C) compared with Sample 5 (425°C). Location was near the inner wall of the tube.

The relatively constant high-temperature strength across all processing conditions is due to the dominant strengthening mechanism at elevated temperature not being dependent on precipitates. The dominant strengthening mechanism is instead solid solution strengthening, mainly from Mg. The degree of solid solution strengthening is not dependent on the grain size or $Al_{11}Ce_3$ particle distribution. Comparing the yield strength of the Al-Ce-Mg alloy with a binary Al-Mg alloy helps to confirm this conclusion, as the binary alloy has a comparable but slightly lower strength at 250°C (Table 2). Additionally, the room temperature ductility of the binary alloy is 2-3 times higher than that of the Al-Ce-Mg alloy. This is partially due to the higher strength of the Al-Ce-Mg alloy (according to the Considère criterion [27]), but may also be caused by fracture of the relatively large $Al_{11}Ce_3$ particles.

The increase in ductility, especially at high temperature, with an increase in APR can also be explained by observing Figure 5. It can be seen, particularly in the highest APR specimen, that the microstructure is somewhat inhomogeneous, with bands of high particle density separated by bands of low particle density. This structure appears similar to rolled sheet or stringers in conventional extrusion. Rolled microstructures often have a strong inhomogeneity of tensile ductility in the rolling direction versus the long transverse direction due to a similar banded structure, with the rolling direction (where the bands are aligned with the tensile direction) giving higher ductility than the transverse directions (where the bands are perpendicular to the tensile direction) [28,29]. Similar observations to those from this study were also made during friction extrusion an Al-12% transition metal alloy, which formed stringers aligned in the extrusion direction. The orientation of these, along with refinement of second phase intermetallics, were found to increase tensile ductility when compared to conventional extrusion [30].

Due to the tubular nature of the extrusions in this work, transverse tensile tests could not be performed to test whether there is significant anisotropy in the ductility of the extruded material. However, due to the rotating nature of the ShAPE process, the actual direction of material flow is not linear. This means that the orientation of these bands of high particle density are not necessarily aligned with the tensile direction; instead, they are aligned in a spiral shape that is dependent on the APR. A high APR is associated with a longer spiral, and therefore the bands of high particle density are more closely aligned with the extrusion (and therefore tensile) direction. The particle band alignment with the tensile direction combined with the hypothesized ductility anisotropy means that the low APR samples with particle bands aligned closer to the tensile direction should have higher tensile ductility than the high APR samples. To confirm this hypothesis, Figure 7 shows two post-tensile samples of the lowest and highest APR (Samples 1 and 5). Note that the failure in the low-APR Trial 1 appears to happen directly along the spiral, which is in the direction perpendicular to the particle bands. By contrast, the high-APR Trial 5 demonstrated a ductile failure that appears similar to a conventionally extruded tube, as the particle bands were aligned closely to the tensile direction and there was very little tensile stress in the direction perpendicular to them.

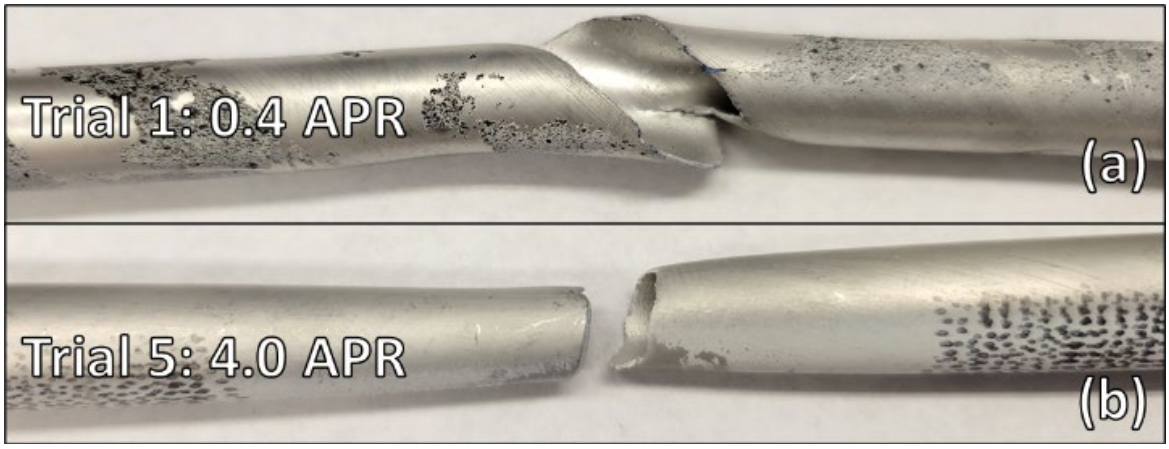

Figure 8: Post-tensile specimens for low and high APR tested at 250°C from Trials 1 and 5, respectively.

5.0 Conclusions

Fabrication of thin-walled tubes from Al-Ce-Mg alloys was achieved using ShAPE, and the product was examined using microscopy and mechanically tested. The following conclusions were drawn:

- ShAPE was found to be a suitable technique for the fabrication of Al-Ce alloy tubing. During processing, the coarse eutectic $Al_{11}Ce_3$ structure was broken up into smaller particles and the grain size was refined.
- The ShAPE-extruded Al-8Ce-4Mg alloy had a 66% higher room temperature yield strength than a binary Al-4Mg alloy. The refined $Al_{11}Ce_3$ particles were effective strengtheners and caused a high degree of strain hardening via Orowan looping.
- The room temperature yield strength and UTS was dependent on the extrusion temperature, as the low temperature extrusions lead to more microstructural refinement. The room temperature ductility was not strongly dependent on processing parameters and was likely limited by fracture of the $Al_{11}Ce_3$ particles.
- The elevated temperature yield strength and UTS was not strongly dependent on processing parameters. It was likely controlled by the Mg solid solution strengthening. The elevated temperature ductility was dependent mainly on the APR due to inhomogeneity in the microstructure leading to anisotropy. Higher APR created bands of precipitates more aligned with the tensile direction, which allowed higher tensile ductility.

6.0 References

[1] V. Raghavan, Al-Ce-Mg (Aluminum-Cerium-Magnesium), J Phs Eqil and Diff 28 (2007) 453–455. https://doi.org/10.1007/s11669-007-9136-4.

[2] K.A. Gschneidner, F.W. Calderwood, The Al−Ce (Aluminum-Cerium) system, Bulletin of Alloy Phase Diagrams 9 (1988) 669–672. https://doi.org/10.1007/BF02883162.

[3] Y. Liu, R.A. Michi, D.C. Dunand, Cast near-eutectic Al-12.5 wt.% Ce alloy with high coarsening and creep resistance, Materials Science and Engineering: A 767 (2019) 138440. https://doi.org/10.1016/j.msea.2019.138440.

[4] K. Sisco, A. Plotkowski, Y. Yang, D. Leonard, B. Stump, P. Nandwana, R.R. Dehoff, S.S. Babu, Microstructure and properties of additively manufactured Al–Ce–Mg alloys, Sci Rep 11 (2021) 6953. https://doi.org/10.1038/s41598-021-86370-4.

[5] T. Wu, A. Plotkowski, A. Shyam, D.C. Dunand, Microstructure and creep properties of cast near-eutectic Al–Ce–Ni alloys, Materials Science and Engineering: A 833 (2022) 142551. https://doi.org/10.1016/j.msea.2021.142551.

[6] R.A. Ayres, Alloying aluminum with magnesium for ductility at warm temperatures (25 to 250°C), Metall Trans A 10 (1979) 849–854. https://doi.org/10.1007/BF02658303.

[7] Z.C. Sims, O.R. Rios, D. Weiss, P.E.A. Turchi, A. Perron, J.R.I. Lee, T.T. Li, J.A. Hammons, M. Bagge-Hansen, T.M. Willey, K. An, Y. Chen, A.H. King, S.K. McCall, High performance aluminum–cerium alloys for high-temperature applications, Mater. Horiz. 4 (2017) 1070–1078. https://doi.org/10.1039/C7MH00391A.

[8] N.A. Belov, E.A. Naumova, D.G. Eskin, Casting alloys of the Al–Ce–Ni system: microstructural approach to alloy design, Materials Science and Engineering: A 271 (1999) 134–142. https://doi.org/10.1016/S0921-5093(99)00343-3.

[9] M. Soleymanpour, H.J. Aval, R. Jamaati, Manufacturing of high-toughness Al–Si alloy by rolling and friction stir processing: Effect of traverse speed, CIRP Journal of Manufacturing Science and Technology 37 (2022) 19–36. https://doi.org/10.1016/j.cirpj.2021.12.007.

[10] Z.Y. Ma, A.L. Pilchak, M.C. Juhas, J.C. Williams, Microstructural refinement and property enhancement of cast light alloys via friction stir processing, Scripta Materialia 58 (2008) 361–366. https://doi.org/10.1016/j.scriptamat.2007.09.062.

[11] M. Riestra, E. Ghassemali, T. Bogdanoff, S. Seifeddine, Interactive effects of grain refinement, eutectic modification and solidification rate on tensile properties of Al-10Si alloy, Materials Science and Engineering: A 703 (2017) 270–279. https://doi.org/10.1016/j.msea.2017.07.074.

[12] A. Plotkowski, O. Rios, N. Sridharan, Z. Sims, K. Unocic, R.T. Ott, R.R. Dehoff, S.S. Babu, Evaluation of an Al-Ce alloy for laser additive manufacturing, Acta Materialia 126 (2017) 507–519. https://doi.org/10.1016/j.actamat.2016.12.065.

[13] W. Wang, Q. Pan, G. Lin, X. Wang, Y. Sun, X. Wang, J. Ye, Y. Sun, Y. Yu, F. Jiang, J. Li, Y. Liu, Microstructure and properties of novel Al-Ce-Sc, Al-Ce-Y, Al-Ce-Zr and Al-Ce-Sc-Y alloy conductors processed by die casting, hot extrusion and cold drawing, Journal of Materials Science & Technology 58 (2020) 155–170. https://doi.org/10.1016/j.jmst.2020.03.073.

[14] C. Zhang, Y. Wang, H. Lv, H. Gao, J. Wang, B. Sun, Enhanced load transfer and ductility in Al–9Ce alloy through heterogeneous lamellar microstructure design by cold rolling and annealing, Materials Science and Engineering: A 821 (2021) 141591. https://doi.org/10.1016/j.msea.2021.141591.

[15] A. Mogucheva, D. Zyabkin, R. Kaibyshev, Effect of the Thermomechanical Processing on Microstructure and Properties of an Al-Ce Alloy, Materials Science Forum 706–709 (2012) 361–366. https://doi.org/10.4028/www.scientific.net/MSF.706-709.361.

[16] P. Vishnu, R. Raj Mohan, E. Krishna Sangeethaa, S. Raghuraman, R. Venkatraman, A review on processing of aluminium and its alloys through Equal Channel Angular Pressing die, Materials Today: Proceedings 21 (2020) 212–222. https://doi.org/10.1016/j.matpr.2019.04.223.

[17] Brandon Scott Taysom, Nicole Overman, Matt Olszta, Md Reza-E-Rabby, Tim Skszek, Massimo DiCiano, Scott Whalen, Shear assisted processing and extrusion of enhanced strength aluminum alloy tubing, Internal Journal of Machine Tools and Manufacture 169 (2021). https://doi.org/10.1016/j.ijmachtools.2021.103798.

[18] S. Whalen, N. Overman, V. Joshi, T. Varga, D. Graff, C. Lavender, Magnesium alloy ZK60 tubing made by Shear Assisted Processing and Extrusion (ShAPE), Materials Science and Engineering: A 755 (2019) 278–288. https://doi.org/10.1016/j.msea.2019.04.013.

[19] S.A. Nazari Tiji, A. Asgharzadeh, T. Park, S.A. Whalen, M. Reza-E-Rabby, M. Eller, F. Pourboghrat, Microstructure and mechanical properties of the AA7075 tube fabricated using shear assisted processing and extrusion (ShAPE), Archiv.Civ.Mech.Eng 21 (2021) 44. https://doi.org/10.1007/s43452-021-00179-6.

[20] X. Ma, E. Nickerson, T. Wang, D. Zhang, T. Pelletiers, S. Whalen, X. Li, Friction extrusion of ODS copper rod made from powder, Journal of Manufacturing Processes 84 (2022) 223–229. https://doi.org/10.1016/j.jmapro.2022.10.003.

[21] T. Wang, J.E. Atehortua, M. Song, M. Reza-E-Rabby, B.S. Taysom, J. Silverstein, T. Roosendaal, D. Herling, S. Whalen, Extrusion of Unhomogenized Castings of 7075 Aluminum via ShAPE, Materials & Design 213 (2022) 110374. https://doi.org/10.1016/j.matdes.2021.110374.

[22] S. Whalen, M. Olszta, Md. Reza-E-Rabby, T. Roosendaal, T. Wang, D. Herling, B.S. Taysom, S. Suffield, N. Overman, High speed manufacturing of aluminum alloy 7075 tubing by Shear Assisted Processing and Extrusion (ShAPE), Journal of Manufacturing Processes 71 (2021) 699–710. https://doi.org/10.1016/j.jmapro.2021.10.003.

[23] S. Whalen, N. Overman, B.S. Taysom, M. Bowden, Md. Reza-E-Rabby, T. Skszek, M. DiCiano, Effect of high iron content on direct recycling of unhomogenized aluminum 6063 scrap by Shear Assisted Processing and Extrusion, Journal of Manufacturing Processes 97 (2023) 115–124. https://doi.org/10.1016/j.jmapro.2023.04.067.

[24] Brian Milligan, Scott Taysom, Ben Schuessler, Tim Roosendaal, Teresa Lemmon, Scott Whalen, UPCYCLING OF MIXED ALUMINUM ALLOY SHREDDER SCRAP USING SHEAR PROCESSING, ASM Advanced Materials and Processes 182 (2024).

[25] L. F. Mondolfo, Aluminum Alloys, Structure and Properties, Butterworths, 1976.

[26] D.R. Satish, D.R. Kumar, M. Merklein, Effect of temperature and punch speed on forming limit strains of AA5182 alloy in warm forming and improvement in failure prediction in finite element analysis: A case study, The Journal of Strain Analysis for Engineering Design 52 (2017) 258–273. https://doi.org/10.1177/0309324717704995.

[27] G.E. Dieter, Mechanical Metallurgy, McGraw-Hill, 1988.

[28] X. Fan, Y. Li, C. Xu, B. Wang, R. Peng, J. Chen, Improved mechanical anisotropy and texture optimization of a 3xx aluminum alloy by differential temperature rolling, Materials Science and Engineering: A 799 (2021) 140278. https://doi.org/10.1016/j.msea.2020.140278.

[29] T.S. Srivatsan, C.W. Meyers, Texture and microstructure contributions to anisotropy in wrought aluminium alloys, J Mater Sci Lett 6 (1987) 326–328. https://doi.org/10.1007/BF01729342.

[30] S. Whalen, M. Olszta, C. Roach, J. Darsell, D. Graff, Md. Reza-E-Rabby, T. Roosendaal, W. Daye, T. Pelletiers, S. Mathaudhu, N. Overman, High ductility aluminum alloy made from powder by friction extrusion, Materialia 6 (2019) 100260. https://doi.org/10.1016/j.mtla.2019.100260.

Pacific Northwest National Laboratory

902 Battelle Boulevard
P.O. Box 999
Richland, WA 99354

1-888-375-PNNL (7665)

www.pnnl.gov